Synthesis of Dialdehyde Cellulose Nanocrystal Hydrogel for Antibiotic Laced Wastewater Remediation

Katherine Zhang

1. Introduction

Necessity for Efficient Wastewater Treatment

The release of hospital, municipal, and industrial wastewater effluent laced with antibiotics have prompted global health concerns [1-3]. Antibiotics are poorly metabolized by humans and animals resulting in 10-90% of consumed antibiotics to be found in wastewater treatment plants, hospital wastewater; and surface and groundwater [4, 5]. Doxycycline Hydrochloride (Doxy), a broad-spectrum antibiotic, will be the target pollutant investigated in this study due to its widespread usage, high environmental toxicity, low biodegradability, and complex molecular structure [6]. Doxy's stable and complex molecular structure make it resistant to oxidizing agents and is thus ineffectively removed by solely using conventional biological wastewater treatments [7].

Additional treatments such as membrane-based separation processes, ion-exchange, coagulation and adsorption have also been applied for the removal of toxins in water, but exhibit the limitation of having a high-cost or being inefficient in removing high concentrations of stable pollutants [8]–[10]. Of these treatments, adsorption shows superior potential due to its efficacy, simple design, and stability to toxic substances [11]. Nanocellulose offers excellent properties as an adsorbent such as high availability, renewability, biodegradability, low-cost, and a highly-ordered cellulose structure with facilitated accessibility to its microstructure [12]–[15]. In particular, cellulose nanocrystals (CNC) exhibits the advantages of conventional cellulosic materials with the addition of large specific surface area, low density, and high mechanical strength which ultimately enhances adsorption efficiency. Additional periodate oxidation of CNC yields dialdehyde cellulose (DCNC), which creates a highly functionalized cellulose

material abundant with aldehyde groups. Based upon the Schiff Base reaction, nitrogen from Doxy's amine groups act as a nucleophile with the carbon from DCNC's carbonyl group to form a C=O group and displaced water molecules [16]. However, a sustainable DCNC material has not been commercialized in wastewater treatment yet due to its dispersion within aqueous solutions which leads to secondary pollution and high regeneration costs [17].

DCNC Hydrogel

To synthesize a sustainable and recoverable adsorbent, DCNC could be combined into a hydrogel network. Hydrogels provide 3D polymeric networks with a crosslinked structure that prevents disintegration and exhibit high stability, which is a vital component preventing the hydrogels from disintegrating during wastewater treatment [18]. For the hydrogel platform, sodium alginate (SA) will be used since it is naturally occurring, anionic, cost-efficient, and easily forms a gel. SA's carboxylic groups also allow for it to be crosslinked with multivalent cations to generate hydrogel beads (Fig. 1) [19]. Thus, the synthesis of a CNC hydrogel adsorbent aims to improve mechanical strength and stability limitations of CNCs and to remediate Doxy from water while efficiently utilizing products that would otherwise be agricultural waste products. Overall, this study looks to synthesize a sustainable and recoverable hydrogel to efficiently remediate Doxy from wastewater.

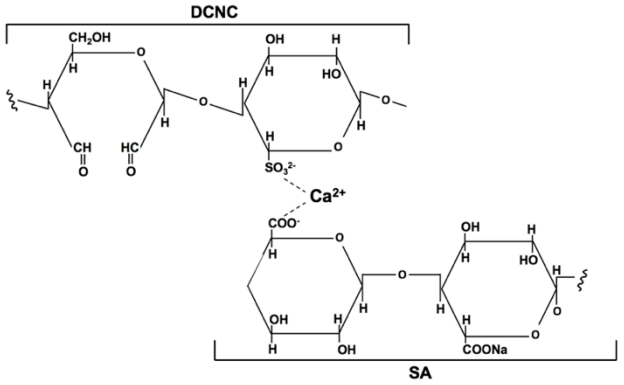

Figure 1. Chemical structure of DCNC-SA. Sulfite groups crosslink with carboxylic acid groups of SA to form hydrogel network.

2. Methodology

DCNC Preparation

DCNC was prepared according to a previously published method [20]. First, CNC (provided by The Process Development Center at the University of Maine) was measured into a media storage bottle covered with aluminum foil. Then, sodium periodate (Alfa Aesar, USA, 7790-21-8) was measured in a beaker with a magnetic stirrer and covered with aluminum foil to prevent the photocatalytic decomposition of sodium periodate [21]. Distilled water was added to the sodium periodate in a dark room and mechanically mixed until homogenous. The sodium periodate mixture was added into the CNC bottle in a dark room at 150 RPM in an oil bath at 54 °C. After 6 hours, the solution was transferred into dialysis membranes (6000 to 8000 Dalton MWCO, Fisher Scientific, USA) for purification and dialysis baths were changed every 2-12 hours. When the conductivity of the dialysis bath was <5 μS/cm for 12 hours, the final DCNC product was centrifuged at 6000 RPM for 10 minutes to remove remaining impurities. The concentration of DCNC was then measured by taking samples of DCNC in aluminum boats and placing them in an oven at 70 °C for 24 hours. Concentration was measured by Eq. (1):

$$CNC\ concentration = \frac{(Initial\ Mass - Al\ boat) - (Final\ mass - Al\ boat)}{(Initial\ Mass\text{-}Al\ boat)} \quad (1)$$

CNC/DCNC Characterization

To confirm the successful preparation of DCNC, the chemical compositions of CNC and DCNC were investigated using a FTIR spectrometer (Nicolet 8700, Thermo Scientific, USA). Then the crystal structures of CNC and DCNC were characterized via X-ray diffraction (XRD; Bruker, Germany) with Kα radiation, Kβ (x2) filter, operating voltage of 40 kV, and operating current of 15 mA.

Preparation of DCNC-SA Hydrogel Beads

DCNC and SA were dissolved in water by vigrously stirring for 30 minutes to obtain a homogenous solution. DCNC to SA ratios of 1.25:2, 1.25:1.25, and 1.25:0.5 as well as pure 2 wt% SA were prepared. The hydrogel mixtures were then loaded into a syringe containing plastic tubing with an inner diameter of 0.2 mm. The syringe was placed into a mechanical syringe pump (Fisher Scientific, USA, 14-831-13) with an ejection speed of 30 mL/hr, stirring speed of 50 RPM, drop height of 10 cm from the surface of 1 mol $CaCl_2$ solution, and 30 min crosslinking time.

DCNC-SA Hydrogel Bead Characterization

To confirm the successful synthesis of DCNC-SA hydrogel beads, the chemical composition of DCNC, SA, and DCNC-SA were compared using a FTIR spectrometer. Then SEM (Phenom Pharos Desktop SEM, Thermo Fisher, USA) images were taken to compare the microstructural morphologies of DCNC-SA and SA. To elucidate surface charges, the zeta potential of CNC, DCNC, SA, and DCNC-SA were measured using a Zetaprobe analyzer (Colloidal Dynamics, USA). Thermogravimetric analysis (TGA) was conducted to compare and elucidate the thermal stability of DCNC, SA, and DCNC-SA.

Adsorption Experiments

Adsorption Isotherm

The adsorption experiments of Doxy on DCNC-SA were conducted using 0.2 g of hydrogel beads in Doxy solutions (pH 7) that ranged from 0 to 4000 ppm placed in a

shaker (180 RPM) for 24 hours at room temperature. After the 24-hour adsorption period, the post-adsorption solutions were diluted until they were between 10-20 ppm and the UV absorbance values (Abs) of each sample were measured by a UV-vis spectrometer (GENYSYS 10S, Thermo Fisher, USA, 840-208100). The concentration of solution (C_e) was calculated where Ab = UV absorbance value, k = standard curve k-value, D = dilution times in Eq. (2):

$$C_e = (Ab/k)*D \qquad (2)$$

The adsorption isotherm data was then fitted using the Langmuir and Freundlich isotherm models [22].

The Langmuir model suggests that the maximum adsorption capacity mechanism occurs in the monolayer of an adsorbate [23].The linear form of the Langmuir isotherm model is represented by the following Eq. (3):

$$(C_e/q_e) = 1/(q_m*K)+(C_e/q_m) \qquad (3)$$

The Freundlich model suggests that the maximum adsorption capacity mechanism occurs in heterogeneous surfaces [24]. The linear form of the Freundlich isotherm model is represented by Eq. (4):

$$ln(q_e) = ln(k) + (1/n)*ln(C_e) \qquad (4)$$

C_e = equilibrium Doxy concentration (mg/L), q_m = maximum adsorption capacity (mg/g), q_e = adsorbed Doxy at equilibrium (mg/g), K = Langmuir constant, l and n = Freundlich constants.

Adsorption Kinetics

The adsorption experiments of Doxy on DCNC-SA were conducted using 0.2 g of hydrogel beads in Doxy solutions (pH 7, 400 ppm) placed in a shaker (180 RPM). The solutions UV absorbance was measured after 5 to 400 minutes. After each adsorption period, the post-adsorption solution was diluted until it was 10-20 ppm to elucidate their UV absorbances. The concentration of the solution was calculated using eq. 1.

The adsorption kinetic data was then fitted using the pseudo-first and pseudo-second models

The pseudo-first order equation suggests that the adsorption reaction follows a physisorption mechanism. The pseudo-first order model is represented by the following equation (5):

$$log(C_e - C_t) = log(C_e) - k_1 t / 2.303 \quad (5)$$

k1 = pseudo first-order constant, t = time, and 2.303 represents ln(10) to convert log to ln.

The pseudo-second order equation suggests that the adsorption reaction follows a chemisorption mechanism. The pseudo-second order model is represented by the following equation (6):

$$t/C_t = 1/(k_2 C_e^2) + t/C_e \quad (6)$$

k_2 = pseudo second-order constant

pH Study

The effect of pH on adsorption was elucidated at pHs ranging from 3 to 11 by adjusting with 0.01 to 3M HCl/NaOH and using a pH meter (FE20, Mettler Toledo, USA). The adsorption experiments of Doxy on DCNC-SA were conducted using 0.2 g of hydrogel beads in Doxy solutions (100 ppm) placed in a shaker (180 RPM). After 24 hours, the post-adsorption solution was diluted until it was 10-20 ppm to measure UV absorbances. Using eq. 1, the final concentration of the solution post-adsorption was calculated. Next, the surface charge densities of DCNC-SA at pHs ranging from 3 to 11 were elucidated using a Zetaprobe analyzer.

Regeneration Study

The reusability of DCNC-SA was elucidated with 30-minute adsorption/desorption periods. After an adsorption period of 30 minutes, a sample of post-adsorption solution was diluted to 10 to 20 ppm and the adsorbate was removed via sieve filtration. The adsorbate was then immersed into 40 mL of 1 to 1 ratio of HCl:Ethanol for desorption and vigorously stirred.

3. Results & Discussions

Chemical Composition Comparison of CNC & DCNC

The chemical composition of CNC and DCNC were first compared using FTIR (Fig. 4). FTIR confirmed that DCNC was successfully synthesized from the periodate oxidation of CNC.

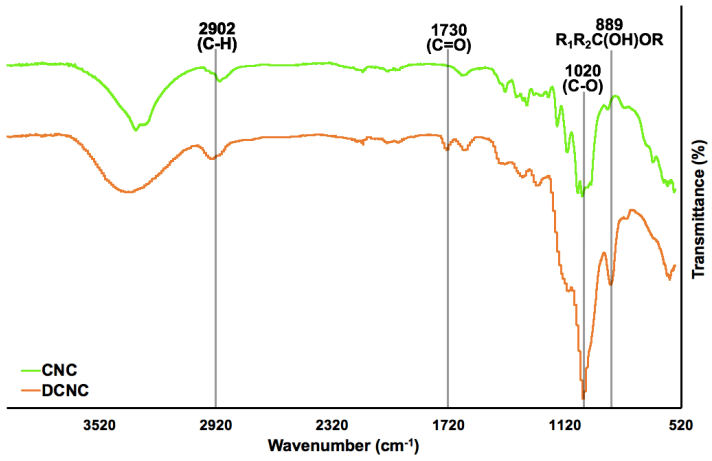

Figure 3. FTIR spectra of CNC & DCNC. FTIR analysis of CNC and DCNC was conducted to confirm the successful synthesis of DCNC. Hemiacetal banding confirmed periodate oxidation of CNC.

From the FTIR, CNC and DCNC had the same peaks in common at 1020 (C-H) and 2902 cm^{-1} (C-O). The FTIR results indicated the cellulose component of the CNC and remained the DCNC [25]. The DCNC has additional peaks at 889 cm^{-1} (hemiacetal groups) and at 1730 (C=O), which indicated the presence of aldehyde groups and thus the successful periodate oxidation of CNC.

Crystallinity Analysis of CNC/DCNC

Next, XRD analysis was used to confirm an effect of periodate oxidation of CNC on the crystallinity of DCNC.

CNC displays crystallinity peaks at 2θ = 14.5° and 22.6°, which indicate the essential crystalline planes of CNC materials [26]. DCNC exhibits no peaks suggesting a decrease in crystallinity from CNC to DCNC and the opening of the CNC glucopyranose rings in order for aldehyde groups to be successfully

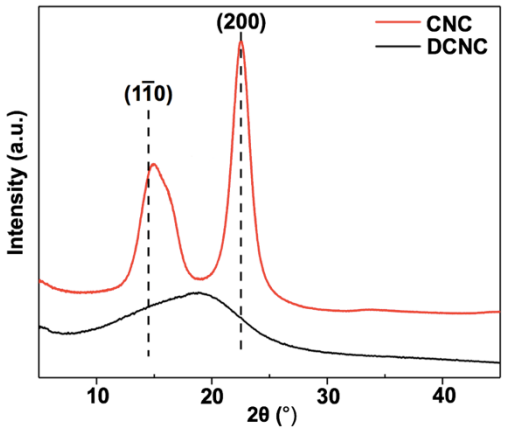

Figure 4. XRD patterns of CNC & DCNC. XRD analysis was used to compare the crystallinity of CNC and DCNC to confirm the successful preparation of DCNC.

Optimal DCNC:SA Hydrogel Preparation

Pure 2wt% SA and DCNC:SA ratios of 1.25:2, 1.25:1.25, and 1.25:0.5 were tested to elucidate the optimal hydrogel ratio for the most effective Doxy removal.

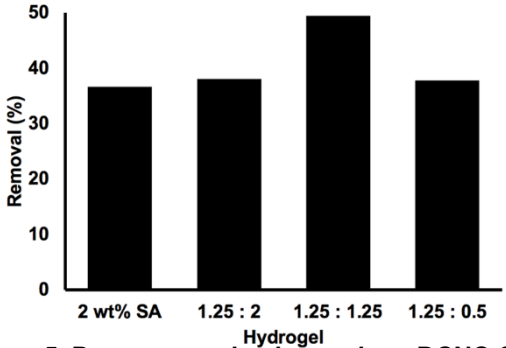

Figure 5. Doxy removal using various DCNC:SA ratios. DCNC wt % stayed constant, varied SA amounts to elucidate the most effective DCNC:SA ratio.

The 1.25:1.25 hydrogel had the highest Doxy removal (48%) after a 1-hour adsorption period and was therefore used for the rest of the study (Fig. 5). A higher DCNC content was expected to correlate with increased Doxy removal based on the Schiff-base reaction, but the decreased SA content resulted in a weak hydrogel network that was unable to sustain the adsorption period.

FTIR of DCNC, SA, and DCNC-SA

FTIR was used to confirm that DCNC-SA hydrogel beads exhibit the chemical characteristics of both DCNC and SA.The hydrogel exhibits peaks at 1594 cm^{-1} and 1408 cm^{-1} that represent the present of carboxyl group, which are distinctive to SA (Fig. 6). The DCNC-SA spectrum shows no peak of C=O bonds of DCNC at 1730 cm^{-1} which indicate that crosslinking of DCNC caused the disappearance of the carbonyl group peaks [27]. Thus, the FTIR chemically confirms that DCNC-SA hydrogel was successfully synthesized.

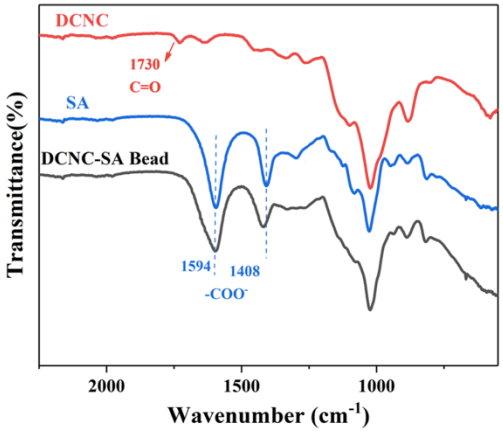

Figure 6. FTIR spectra of DCNC, SA & SA-DCNC. Transmittance bands confirm successful synthesis of SA-DCNC beads

SEM of DCNC-SA vs. pure SA

DCNC-SA and SA surface and cross-section microstructures were analyzed via SEM.

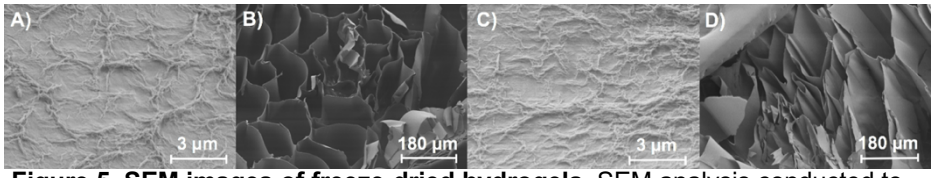

Figure 5. SEM images of freeze-dried hydrogels. SEM analysis conducted to compare morphology of A) DCNC-SA surface and B) cross-section & C) 2 wt% SA surface & D) 2 wt% SA cross-section.

The direct surface of the 2 wt% SA and DCNC-SA qualitatively have a similar undulancy (Fig. 5A & 5C). The cross-section of DCNC-SA qualitatively is more porous than SA's

indicating that the SA being crosslinked with DCNC aided in a more organized pore structure of the hydrogel structure [27] (Fig. 5B & 5D).

Zeta potential of CNC, SA, DCNC, and DCNC-SA

The surface charge densities of CNC, SA, DCNC, and DCNC-SA were elucidated using zeta potential analysis. The zeta potential of CNC was -147.35 mV and for DCNC was -27.96 mV, which indicates a decrease in negativity (Fig. 6). DCNC-SA's zeta potential of -51.01 mV was analyzed to be in between the surface charge density of DCNC (-27.96 mV) and SA (-96.73 mV) [28]. The decreased negativity from SA to DCNC-SA further confirms that DCNC sulfite groups aided in crosslinking with carboxyl groups of SA.

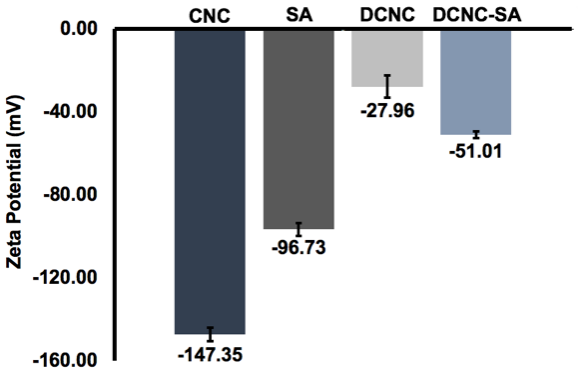

Figure 6. Zeta potential values of CNC, SA, DCNC, and DCNC-SA. Surface charge becomes less negative from CNC to DCNC. Surface charge of DCNC-SA is in between the surface charges of DCNC and SA.

Thermogravimetric Analysis (TGA) of DCNC, SA, and DCNC-SA

To investigate the thermal stability properties of the hydrogel bead, TGA was conducted for DCNC, SA, and DCNC-SA. A strong SA weight % dip occurs at about 200 degrees Celsius and DCNC-SA has a dip that isn't as large as SA's and not as mellow as DCNC's weight % dip (Fig. 7) [29]. At the final temperature of 800 degrees Celsius, DCNC-SA exhibits the most weight (%) and

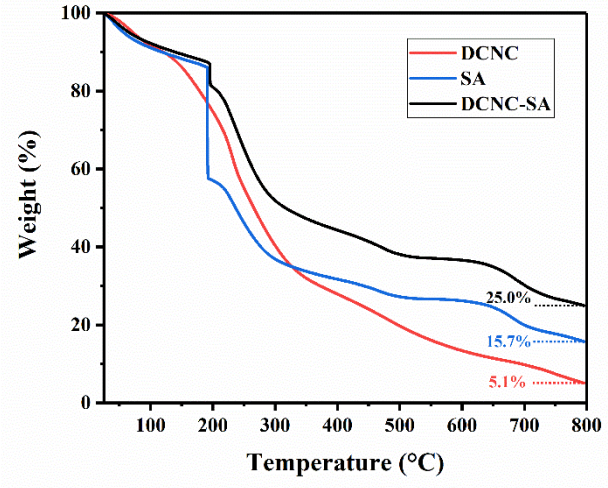

Figure 7. A) Thermogravimetric Analysis (TGA) of DCNC, SA & DCNC-SA & B) Differential thermal gravity (DTG) curves. TGA/DTG indicates DCNC-SA has the highest thermal

thus is the most thermally stable [20], [30]. The TGA confirms that crosslinking attributed to the high stability of DCNC-SA (when compared to DCNC and SA). As the zeta potential (Fig. 6) indicated that DCNC's aldehyde groups may have helped crosslink SA, TGA/DTG can confirm its high crosslinking degree.

Adsorption Isotherm

Adsorption capacities of DCNC-SA were then elucidated by fitting the data of adsorption (mg/g) with the Langmuir and Freundlich models [29], [31][32].

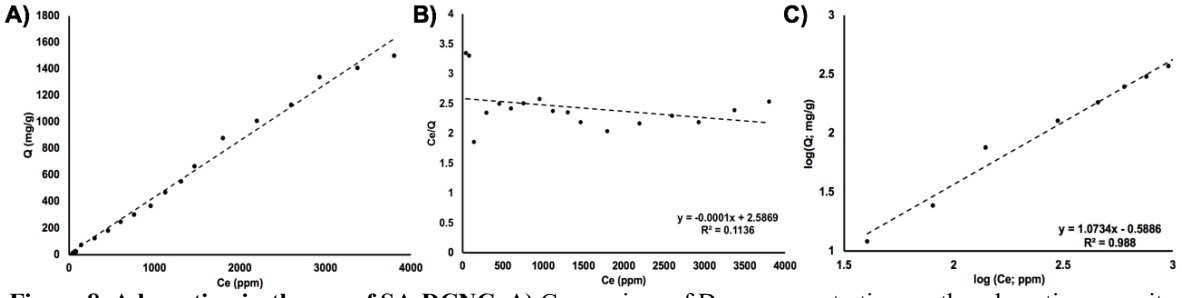

Figure 8. Adsorption isotherms of SA-DCNC. A) Comparison of Doxy concentration vs. the adsorption capacity, **B)** Isotherm fitted using the Langmuir model and **C)** Freundlich model.

The adsorption isotherm data (Fig. 8A) was fitted using the Langmuir (R^2 = 0.114) and Freundlich models (R^2 = 0.988). Since the R^2 value for the Freundlich model is closer to 1 than the Langmuir R^2 value, the Freundlich model was used to explain a factor of adsorption mechanism (Fig. 8. B-C). The Freundlich model suggests that the adsorption mechanism of Doxy occurs on heterogenous surfaces. DCNC-SA can adsorb Doxy on various layers which allows high-concentration adsorption to occur [33].

Adsorption kinetics

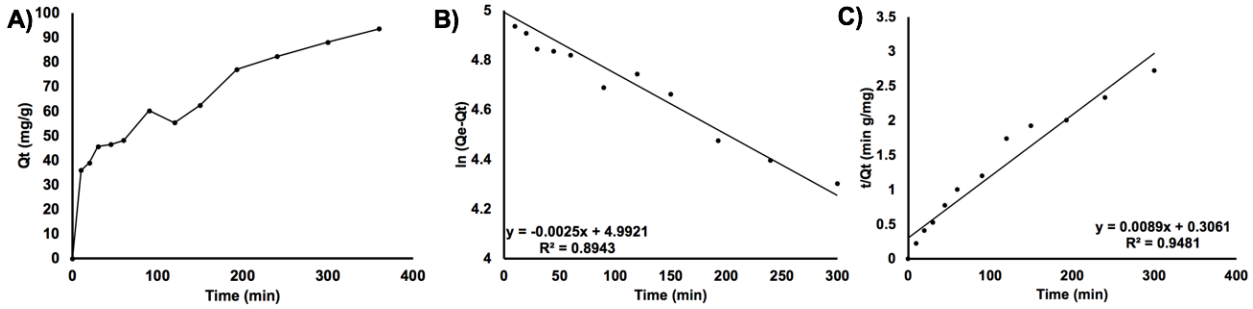

Figure 9. Adsorption kinetics of SA-DCNC. A) Time vs. adsorption uptake & Adsorption fitted using the **B)** pseudo-first and **C)** pseudo-second models.

Adsorption kinetics were fitted using the pseudo-first (R^2 = .8943) and pseudo-second models (R^2 = .9481). Since the R^2 value of the pseudo-second model is closer to 1, it can be used to elucidate another factor of DCNC-SA's adsorption mechanism. The pseudo-second model suggests that chemisorption is another adsorption mechanism of DCNC-SA. The Schiff-base reaction occurs between aldehyde groups of DCNC and amino groups of Doxy rather than weak van der Waal's forces.

Effect of pH on adsorption

To elucidate the effect of pH on DCNC-SA's adsorption capacities, Doxy removal and the zeta potential of DCNC-SA was measured from pH 2 to 12. The increasing absolute value of zeta potential of the DCNC-SA as pH increases indicates that the hydrogel becomes more negative correlating to more active sites

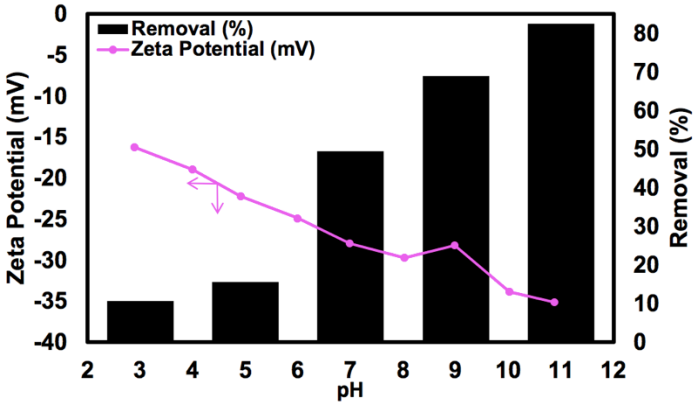

Figure 10. Effect of Doxy pH on adsorption and zeta potential. Removal efficiency increased as pH increased and absolute value of zeta potential increased.

for Doxy adsorption and thus higher removal % (Fig. 10) [34]. The abundant sulfite groups of DCNC and aldehyde groups exposed on DCNC-SA's surface interacted with OH- groups to increase Doxy removal efficiency as pH increased [35].

Hydrogel reusability

The adsorption (Q_e) was measured using the same sample regenerated 3 times to elucidate the reusability properties of DCNC-SA.

The Q_e values indicate adsorption ranges from 30 to 45 mg/g within 3 regeneration cycles, in which at lowest, regeneration cycle 2 loses 33% efficiency. However, the hydrogels may not have been fully desorbed before the second regeneration cycle leading to low adsorption. (A future study will replicate this test to obtain better results)

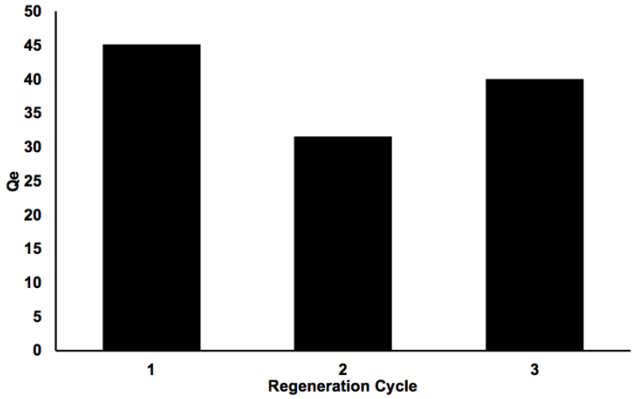

Figure 11. Adsorption at different DCNC-SA regeneration cycles. The adsorption capacity after 3 regeneration cycles remains in a close range to the first regeneration cycle.

Dosage Study

Hydrogel dosage were studied from 0.02 to 0.5g to measure Doxy removal percent and Q_e (mg/g).As hydrogel dosage increases from 0.02 to 0.5g, removal % increases from 30 to 68% while Q_e decreases from 880 mg/g to 60 mg/g (Fig. 12). An increased quantity of active sites was available as dosage increase which lead to increased Doxy removal %. However, since there are more active sites, but the same concentration of Doxy, the adsorption per gram of adsorbent decreases.

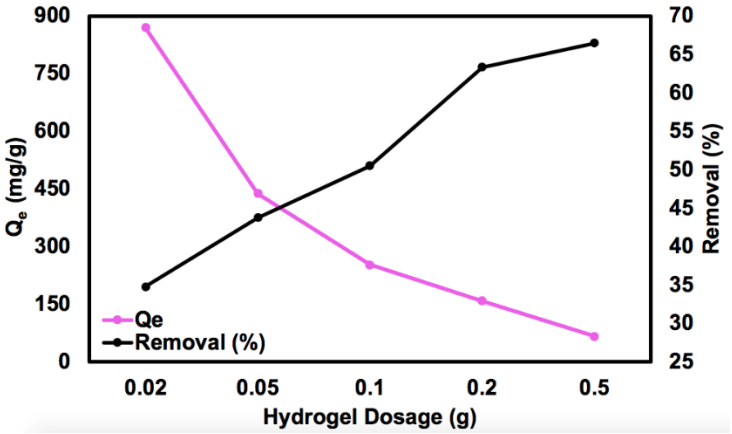

Figure 15. Effect of hydrogel dosage on adsorption efficacy. Removal % of Doxy increases as hydrogel dosage increases.

4. Conclusions

This study successfully synthesized DCNC-SA hydrogel beads with a highly efficient Doxy removal rate with a sustainable and simple approach consisting of mechanically pumping a homogenous mixture of DCNC-SA into 1M $CaCl_2$ solution for crosslinking. The DCNC to SA ratio of 1.25:1.25 exhibited optimal Doxy removal (48%). The DCNC-SA hydrogel beads reached a maximum adsorption capacity of 1500.1 mg/g during the adsorption isotherm. Adsorption mechanisms of DCNC-SA include adsorption taking place on heterogenous surfaces as explained by the Freundlich equation and chemisorption as explained by the pseudo-second order equation when analyzing adsorption isotherm and kinetics, respectively. The DCNC-SA hydrogel beads exhibited increasing Doxy removal as pH increased. The regeneration study indicated that DCNC-SA could easily be regenerated for at least 3 cycles and recovered, which addresses previous limitations of nanocellulose applications within wastewater treatment. Overall, DCNC-SA is a promising adsorbent to remediate Doxy

Moreover, future research will investigate optimizing DCNC-SA adsorption rates of Doxy and extending applications in wastewater treatment to dye remediation [20]. Additionally, DCNC-SA is biocompatible allows research to be extended to explore biomedical applications such as for drug delivery through in vitro drug release experiments [36].

References

[1] E. Sanganyado and W. Gwenzi, “Antibiotic resistance in drinking water systems: Occurrence, removal, and human health risks,” *Sci. Total Environ.*, vol. 669, pp. 785–797, Jun. 2019.

[2] M.-C. Danner, A. Robertson, V. Behrends, and J. Reiss, “Antibiotic pollution in surface fresh waters: Occurrence and effects,” *Sci. Total Environ.*, vol. 664, pp. 793–804, May 2019.

[3] Z. Xu, T. Li, J. Bi, and C. Wang, “Spatiotemporal heterogeneity of antibiotic pollution and ecological risk assessment in Taihu Lake Basin, China,” *Sci. Total Environ.*, vol. 643, pp. 12–20, Dec. 2018.

[4] E. O’Flaherty and E. Cummins, “Antibiotic resistance in surface water ecosystems: Presence in the aquatic environment, prevention strategies, and risk assessment,” *Hum. Ecol. Risk Assess. An Int. J.*, vol. 23, no. 2, pp. 299–322, Feb. 2017.

[5] C. M. Manaia *et al.*, “Antibiotic resistance in wastewater treatment plants: Tackling the black box,” *Environ. Int.*, vol. 115, pp. 312–324, Jun. 2018.

[6] S. Liu *et al.*, “Facile synthesis of Cu(II) impregnated biochar with enhanced adsorption activity for the removal of doxycycline hydrochloride from water,” *Sci. Total Environ.*, vol. 592, pp. 546–553, Aug. 2017.

[7] F. Salvador, N. Martin-Sanchez, R. Sanchez-Hernandez, M. J. Sanchez-Montero, and C. Izquierdo, “Regeneration of carbonaceous adsorbents. Part I: Thermal Regeneration,” *Microporous Mesoporous Mater.*, vol. 202, pp. 259–276, Jan. 2015.

[8] Y. Zheng *et al.*, “Thermodynamic analysis of high-pressure methane adsorption on coal-based activated carbon,” *Fuel*, vol. 230, pp. 172–184, Oct. 2018.

[9] M. Naushad *et al.*, “Efficient removal of toxic phosphate anions from aqueous environment using pectin based quaternary amino anion exchanger,” *Int. J. Biol. Macromol.*, vol. 106, pp. 1–10, Jan. 2018.

[10] K. Rambabu *et al.*, “Effective treatment of dye polluted wastewater using nanoporous CaCl2 modified polyethersulfone membrane,” *Process Saf. Environ. Prot.*, vol. 124, pp. 266–278, Apr. 2019.

[11] N. Mohammed, N. Grishkewich, H. A. Waeijen, R. M. Berry, and K. C. Tam, “Continuous flow adsorption of methylene blue by cellulose nanocrystal-alginate hydrogel beads in fixed bed columns,” *Carbohydr. Polym.*, vol. 136, pp. 1194–1202, Jan. 2016.

[12] P. Chen, X. Liu, R. Jin, W. Nie, and Y. Zhou, “Dye adsorption and photo-induced recycling of hydroxypropyl cellulose/molybdenum disulfide composite hydrogels,” *Carbohydr. Polym.*, vol. 167, pp. 36–43, Jul. 2017.

[13] C. Liu, A. M. Omer, and X. Ouyang, “Adsorptive removal of cationic methylene blue dye using carboxymethyl cellulose/k-carrageenan/activated montmorillonite composite beads: Isotherm and kinetic studies,” *Int. J. Biol. Macromol.*, vol. 106, pp. 823–833, Jan. 2018.

[14] N. Lin, A. Gèze, D. Wouessidjewe, J. Huang, and A. Dufresne, “Biocompatible Double-Membrane Hydrogels from Cationic Cellulose Nanocrystals and Anionic Alginate as Complexing Drugs Codelivery,” *ACS Appl. Mater. Interfaces*, vol. 8, no. 11, pp. 6880–6889, Mar. 2016.

[15] R. J. Moon, G. T. Schueneman, and J. Simonsen, “Overview of Cellulose Nanomaterials, Their Capabilities and Applications,” *JOM*, vol. 68, no. 9, pp. 2383–2394, Sep. 2016.

[16] P. E. Wall, “CHROMATOGRAPHY: THIN-LAYER (PLANAR) | Spray Reagents,”

Encycl. Sep. Sci., pp. 907–915, Jan. 2000.
[17] L. Obeid *et al.*, "Adsorption of a cationic surfactant by a magsorbent based on magnetic alginate beads," *J. Colloid Interface Sci.*, vol. 432, pp. 182–189, Oct. 2014.
[18] B. Bethi, V. Manasa, K. Srinija, and S. H. Sonawane, "Intensification of Rhodamine-B dye removal using hydrodynamic cavitation coupled with hydrogel adsorption," *Chem. Eng. Process. - Process Intensif.*, vol. 134, pp. 51–57, Dec. 2018.
[19] Y. Lin *et al.*, "A 'signal-on' chemiluminescence biosensor for thrombin detection based on DNA functionalized magnetic sodium alginate hydrogel and metalloporphyrinic metal-organic framework nanosheets," *Talanta*, vol. 207, p. 120300, Jan. 2020.
[20] C.-Q. Ruan, M. Strømme, and J. Lindh, "Preparation of porous 2,3-dialdehyde cellulose beads crosslinked with chitosan and their application in adsorption of Congo red dye," *Carbohydr. Polym.*, vol. 181, pp. 200–207, Feb. 2018.
[21] M. Yao, Z. Wang, Y. Liu, G. Yang, and J. Chen, "Preparation of dialdehyde cellulose graftead graphene oxide composite and its adsorption behavior for heavy metals from aqueous solution," *Carbohydr. Polym.*, vol. 212, pp. 345–351, May 2019.
[22] M. Açıkyıldız, A. Gürses, K. Güneş, and D. Yalvaç, "A comparative examination of the adsorption mechanism of an anionic textile dye (RBY 3GL) onto the powdered activated carbon (PAC) using various the isotherm models and kinetics equations with linear and non-linear methods," *Appl. Surf. Sci.*, vol. 354, pp. 279–284, Nov. 2015.
[23] U. Jinendra, D. Bilehal, B. M. Nagabhushana, K. R. Reddy, C. V. Reddy, and A. V. Raghu, "Template-free hydrothermal synthesis of hexa ferrite nanoparticles and its adsorption capability for different organic dyes: Comparative adsorption studies, isotherms and kinetic studies," *Mater. Sci. Energy Technol.*, vol. 2, no. 3, pp. 657–666, Dec. 2019.
[24] A. Di Paola, E. García-López, G. Marcì, and L. Palmisano, "A survey of photocatalytic materials for environmental remediation," *J. Hazard. Mater.*, vol. 211–212, pp. 3–29, Apr. 2012.
[25] F. Wang *et al.*, "Adsorption and recycling of Cd(II) from wastewater using straw cellulose hydrogel beads," *J. Ind. Eng. Chem.*, Aug. 2019.
[26] M. Aguayo *et al.*, "Isolation and Characterization of Cellulose Nanocrystals from Rejected Fibers Originated in the Kraft Pulping Process," *Polymers (Basel).*, vol. 10, no. 10, p. 1145, Oct. 2018.
[27] U.-J. Kim, S. Kimura, and M. Wada, "Highly enhanced adsorption of Congo red onto dialdehyde cellulose-crosslinked cellulose-chitosan foam," *Carbohydr. Polym.*, vol. 214, pp. 294–302, Jun. 2019.
[28] F. Xiao, X. Guo, J. Li, H. Sun, H. Zhang, and W. Wang, "Electrospinning preparation and dye adsorption capacity of TiO2@Carbon flexible fiber," *Ceram. Int.*, vol. 45, no. 9, pp. 11856–11860, Jun. 2019.
[29] V. P. Mahida and M. P. Patel, "Removal of some most hazardous cationic dyes using novel poly (NIPAAm/AA/N-allylisatin) nanohydrogel," *Arab. J. Chem.*, vol. 9, no. 3, pp. 430–442, May 2016.
[30] M. Ashkani, H. Bouhendi, K. Kabiri, and M. R. Rostami, "Synthesis of poly (2-acrylamido-2-methyl propane sulfonic acid) with high water absorbency and absorption under load (AUL) as concrete grade superabsorbent and its performance," *Constr. Build. Mater.*, vol. 206, pp. 540–551, May 2019.
[31] R. K. Sharma and R. Kumar, "Functionalized cellulose with hydroxyethyl methacrylate

and glycidyl methacrylate for metal ions and dye adsorption applications," *Int. J. Biol. Macromol.*, vol. 134, pp. 704–721, Aug. 2019.
[32] H. Zhang, A. M. Omer, Z. Hu, L.-Y. Yang, C. Ji, and X. Ouyang, "Fabrication of magnetic bentonite/carboxymethyl chitosan/sodium alginate hydrogel beads for Cu (II) adsorption," *Int. J. Biol. Macromol.*, vol. 135, pp. 490–500, Aug. 2019.
[33] J. Wang, X. Meng, Z. Yuan, Y. Tian, Y. Bai, and Z. Jin, "Acrylated Composite Hydrogel Preparation and Adsorption Kinetics of Methylene Blue," *Molecules*, vol. 22, p. 1824, Oct. 2017.
[34] A. Pourjavadi, S. Barzegar, and G. R. Mahdavinia, "MBA-crosslinked Na-Alg/CMC as a smart full-polysaccharide superabsorbent hydrogels," *Carbohydr. Polym.*, vol. 66, no. 3, pp. 386–395, 2006.
[35] D. Yu, Y. Wang, M. Wu, L. Zhang, L. Wang, and H. Ni, "Surface functionalization of cellulose with hyperbranched polyamide for efficient adsorption of organic dyes and heavy metals," *J. Clean. Prod.*, vol. 232, pp. 774–783, Sep. 2019.
[36] Q. Xu, Y. Ji, Q. Sun, Y. Fu, Y. Xu, and L. Jin, "Fabrication of Cellulose Nanocrystal/Chitosan Hydrogel for Controlled Drug Release," *Nanomaterials*, vol. 9, no. 2, p. 253, Feb. 2019.